



Elastometry of deflated capsules elastic moduli from shape and wrinkle analysis

by

**Sebastian Knoche
Dominic Vella
Elodie Aumaitre
Patrick Degen
Heinz Rehage
Pietro Cicuti
Jan Kierfeld**

Elastometry of Deflated Capsules: Elastic Moduli from Shape and Wrinkle Analysis

Sebastian Knoche,¹ Dominic Vella,² Elodie Aumaitre,³ Patrick Degen,⁴ Heinz Rehage,⁴ Pietro Cicuta,³ and Jan Kierfeld¹

¹*Department of Physics, Technische Universität Dortmund, 44221 Dortmund, Germany*

²*OCCAM, Mathematical Institute, 24-29 St Giles', Oxford, OX1 3LB, UK*

³*Cavendish Laboratory, University of Cambridge, JJ Thomson Avenue, CB3 0HE Cambridge, UK*

⁴*Department of Chemistry, Technische Universität Dortmund, 44221 Dortmund, Germany*

Elastic capsules, prepared from droplets or bubbles attached to a capillary (as in a pendant drop tensiometer), can be deflated by suction through the capillary. We study this deflation and show that a combined analysis of the shape and wrinkling characteristics enables us to determine the elastic properties *in situ*. Shape contours are analyzed and fitted using shape equations derived from nonlinear membrane-shell theory to give the elastic modulus, Poisson ratio and stress distribution of the membrane. We include wrinkles, which generically form upon deflation, within the shape analysis. Measuring the wavelength of wrinkles and using the calculated stress distribution gives the bending stiffness of the membrane. We illustrate this method on two very different capsule materials: polymerized octadecyltrichlorosilane (OTS) capsules and hydrophobin (HFBII) coated bubbles. Our results are in agreement with the available rheological data. For hydrophobin coated bubbles the method reveals an interesting nonlinear behavior consistent with the hydrophobin molecules having a rigid core surrounded by a softer shell.

PACS numbers: 62.20.de, 68.05.-n 83.85.-c 46.70.De,

Elastic capsules are ubiquitous in nature as red blood cells, bacterial or virus capsids, and synthetic capsules play an important role in numerous technological applications, including drug delivery and release systems. For stability and applications, the elastic properties of the capsules are crucial, and techniques for the mechanical characterization of single capsules have received much attention (see Ref. [1] for a recent review). However, only very few non-contact techniques are available, and those that are require motion in a surrounding fluid (e.g. shape analysis in shear flow [2] and spinning drop rheometry [3]).

Synthetic capsules can be fabricated by various methods [4], many of which are based on reactions at interfaces such as polymerization or the adsorption of surfactants [5]. The latter techniques can be applied to enclose a drop or bubble emerging from a capillary within an elastic membrane. A pendant capsule produced in this way can then be deformed in order to analyze its elastic response. Because of the simplicity of this procedure, various membrane materials have been studied in this geometry [6–9]. The analysis of those experiments, however, used models developed for pendant drop tensiometry, a technique widely used to determine the surface tension of *liquid-liquid interfaces* by fitting the drop shape to that predicted by the Laplace-Young equation [10]. This technique is not, however, valid for elastic capsules, since it neglects the elastic stresses within the membrane.

In this Letter, we present a non-contact elastometry method for individual capsules, inspired by the pendant drop method but adjusting the theoretical model to account for elasticity. Elastic capsules that are attached to a capillary are deflated by sucking some of the enclosed

medium back into the capillary. We describe deflated shapes (see Fig. 1 for examples) using shell theory for axisymmetric membranes and accounting for the wrinkling induced by deflation. By analyzing the capsule's shape and wrinkling pattern, we can determine its elastic properties, namely the surface Young modulus Y_{2D} , describing the membrane's resistance to stretching, and the Poisson ratio ν_{2D} describing the lateral contraction upon stretching. By adjusting these parameters, the theoretical capsule contour can be fitted to the observed shape (Figs. 1(a) and (b)), and the elastic moduli of the membrane can be determined over a whole range of capsule volumes.

The determination of the membrane's bending stiffness E_B represents another challenge for elastic capsules because it only has a small influence on the capsule contour on large scales and, thus, cannot be obtained by the fitting. Therefore, we combine the shape analysis described above with an analysis of the wrinkles that generically form during deflation, and deduce the bending stiffness from the wavelength of the wrinkles [11]. This combined approach enables us to determine all elastic constants of individual capsules *in situ* from images of the initial and deflated capsule, thus offering a valuable alternative to rheology in planar geometries. In particular, the capsules studied here have a geometry similar to that of capsules used in applications in pharmacy or industry.

We model the capsule as an elastic membrane covering a droplet or bubble, which is attached to a capillary. We neglect the bending resistance for simplicity. The axisymmetric reference configuration (Fig. 1(c), left) is assumed to be free of elastic stresses; the capsule shape is determined by the balance between an isotropic inter-

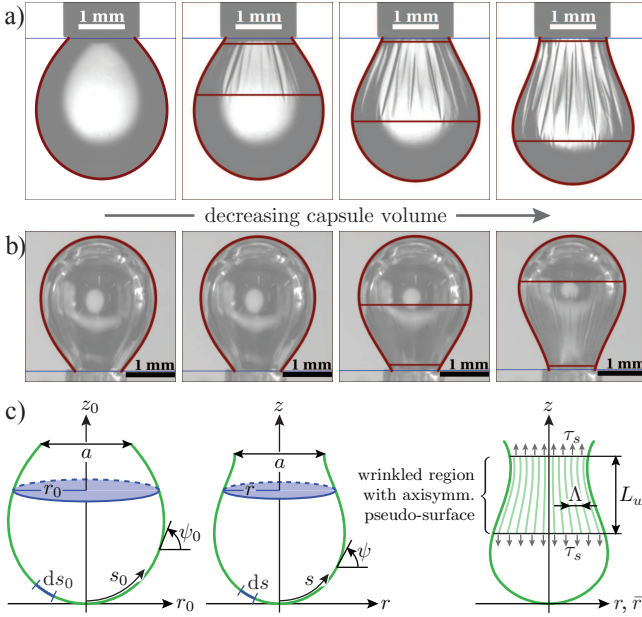


Figure 1: (Color online) (a) and (b) Comparison between fitted contour (solid curve) and original image for OTS (a) and HFBII (b) capsules. The first image shows the equilibrated capsule, while the next three show increasing levels of deflation. The extent of the wrinkled region predicted by the model is shown by the horizontal lines. (c) Arc-length parametrizations in cylindrical coordinates of the undeformed $(r_0(s_0), z_0(s_0))$, deformed $(r(s), z(s))$ and wrinkled midsurface (from left to right). The local stretches in the meridional and hoop directions are given by $\lambda_s = ds/ds_0$ and $\lambda_\phi = r/r_0$, respectively. At the upper rim, a boundary condition fixes the capsule radius to the inner radius of the capillary, $a/2$.

facial tension γ and gravity, which is described by the Laplace-Young equation [12]. We make this assumption because the elastic capsule is formed in this initial state from a fluid interface.

Upon deflation, the capsule changes to an axisymmetric deformed configuration (Fig. 1(c), middle). The local deformation is measured by the meridional and hoop stretches λ_s and λ_ϕ (see Fig. 1(c)) and leads to elastic tensions. For the meridional tension we assume a Hookean constitutive relation [13, 14]

$$\tau_s = \frac{Y_{2D}}{1 - \nu_{2D}^2} \frac{1}{\lambda_\phi} [(\lambda_s - 1) + \nu_{2D}(\lambda_\phi - 1)] + \gamma \quad (1)$$

with the surface Young modulus Y_{2D} (which is related to the bulk Young modulus Y_{3D} and membrane thickness H_0 by $Y_{2D} = Y_{3D}H_0$) and Poisson ratio ν_{2D} . The constitutive law for the hoop tension τ_ϕ is obtained by interchanging all indices s and ϕ . An equilibrium capsule configuration has to satisfy the force balance equations [13]

$$0 = -\frac{\cos \psi}{r} \tau_\phi + \frac{1}{r} \frac{d(r \tau_s)}{ds} \quad (2)$$

$$p - \Delta \rho g z = \kappa_\phi \tau_\phi + \kappa_s \tau_s.$$

Here, p is the pressure at the capsule apex and $\Delta \rho g z$ is the pressure contribution caused by the density difference between the inner and outer fluids. The principal curvatures are denoted by κ_s and κ_ϕ , and the slope angle ψ is defined in Fig. 1(c).

If the capsule is deflated sufficiently, regions with compressive hoop stress (i.e., $\tau_\phi < 0$) develop and wrinkles form in order to release this stress which a membrane with small bending modulus cannot support [15–18]. For highly developed wrinkles the hoop stress is almost completely relaxed [15], and so we modify the shape equations by setting $\tau_\phi = 0$ in the wrinkled region. Assuming wrinkles of small amplitude, the membrane can be described by an axisymmetric pseudo-surface with radial coordinate $\bar{r}(s)$ around which the wrinkled non-axisymmetric midsurface fluctuates [13, 19]. Using the condition $\tau_\phi = 0$ in eq. (1) to find $\lambda_\phi(\lambda_s)$ we then obtain a modified expression for τ_s in the wrinkled region in terms of λ_s , in which λ_ϕ is eliminated [19]. This allows us to obtain a closed set of modified shape equations in the wrinkled region by applying the axisymmetric force balance (2) to the pseudo-surface. Theoretical axisymmetric shapes obtained from integrating eqs. (2) can then be fitted to experimental images by varying the two material parameters Y_{2D} and ν_{2D} and the pressure p .

We have not included a bending energy in this model, because for thin membranes with a bending modulus $E_B \propto Y_{2D}H_0^2$ the bending moments give only small corrections in the shape equations (2). These corrections are controlled by the dimensionless parameter $E_B/\gamma a^2$. Using $a \sim 1$ mm as the capillary diameter, we find that this parameter is only of the order of 10^{-6} for OTS and 10^{-10} for HFBII capsules. Therefore, E_B cannot be inferred directly from an analysis of the capsule's contour.

The shape equations can predict the regions where wrinkles will occur, but not their amplitude and wavelength. These characteristics are mainly determined by the bending modulus E_B of the membrane. Cerda and Mahadevan showed that wrinkles of length L_w in an elastic membrane under longitudinal tension τ_s and some imposed transversal compression will have wavelength [11] (see Fig. 1(c), on the right)

$$\Lambda = (16\pi^2 L_w^2 E_B / \tau_s)^{1/4}. \quad (3)$$

In [19] we show that this result can be adapted to wrinkles on capsules by using the same approach of minimizing the sum of bending and stretching energies.

Based on the theory presented above, a three step fitting procedure can be used in order to determine the elastic moduli of the capsule membrane:

1. The undeformed capsule shape is fitted using the Laplace-Young equation with the interfacial tension γ and the pressure p_0 inside the capsule as free parameters.

2. Shape analysis: Solutions of the shape equations (2) are fitted to images of the deflated capsule with p , ν_{2D} and $K_{2D} = Y_{2D}/2(1 - \nu_{2D})$ (area compression modulus) as free parameters.
3. Wrinkle analysis: The wavelength Λ in the center of the wrinkled region is measured from images. The height L_w of the wrinkled region and a mean value of τ_s over this region are obtained from the fitted solution to the shape equations. Then, the bending modulus E_B is determined from eq. (3). Using the relationship $E_B = Y_{2D}H_0^2/12(1 - \nu_{2D}^2)$ from classical plate theory [20] the corresponding membrane thickness H_0 can be estimated [29].

Note that the position and height L_w of the wrinkled region are *not* fit parameters but are determined from the shape equations and can be used as an independent check. Technical details of the fitting procedure and the underlying image analysis are contained in the Supplementary Material [19].

We tested this procedure by applying it to fit numerically generated deflated capsule shapes with fixed elastic moduli [19]. Furthermore, we compared the results of our analysis to the usual Laplace-Young analysis used in the literature [6–8], in which elastic capsules are fitted with the Laplace-Young equation to obtain the interfacial tension γ and capsule surface A over the course of the deflation. Usually, the Gibbs elastic modulus $E_{\text{Gibbs}} = A d\gamma/dA$ is then calculated from these values. We found that E_{Gibbs} is significantly smaller than the real area compression modulus (see [19] for a diagram). This explains the observations of Stanimirova et. al. that pendant drop tensiometry gives wrong results if applied to capsules with high surface elasticity [7].

We now demonstrate this method on two rather different types of capsules: polymerized OTS capsules and bubbles coated with an interfacial monolayer film of the protein hydrophobin.

To prepare a pendant capsule, a glass cell is filled with p-xylene containing OTS. Then a drop of water is placed into this phase using a syringe. The polymerization process starts immediately after the oil/water-interface is formed. Hydrophobin coated bubbles are prepared in a very similar fashion. As described in previous work [21], an air bubble is placed into a solution of HFBII in water using a J-shaped needle and HFBII molecules adsorb at the interface over the course of 20 minutes. After equilibration, the capsules are deflated slowly by sucking the enclosed medium back into the syringe. The OTS capsule is subsequently re-inflated to check whether the deformation is reversible.

For both systems, several images of the undeformed reference configurations are fitted to the solution of the Laplace-Young equation. The results are averaged to obtain the surface tension $\gamma = 11.2 \text{ mN/m}$ for OTS and

$\gamma = 49.8 \text{ mN/m}$ for HFBII. Both values are lower than the respective values of the clean interfaces.

Deflated capsule configurations with varying volume are fitted using the elastic model. Fig. 2(a) shows the results for an OTS capsule. All data points in Fig. 2(a) represent wrinkled shapes, because even the slightest deformation gives rise to wrinkles due to the low initial surface tension and high compression modulus. We find an area compression modulus K_{2D} which decreases with decreasing V/V_0 . Although the error bars in Fig. 2(a) are overlapping, this result is reliable because the error bars represent worst case systematic errors [19]. The deformation is not perfectly reversible, and we observe hysteresis: The area compression modulus obtained for re-inflated capsules is lower (lower red vs. upper blue data points in Fig. 2(a)). The presence of hysteresis indicates that the decreasing modulus is not an artefact of the method but a result of creep, for example by viscous effects, i.e. breakage or rearrangement of bonds in the OTS network, or by the formation of microdefects such as shear cracks. The video in the supplement [19] shows, however, that computed contours with the moduli fixed to the small-deformation values $K_{2D} \approx 500 \text{ mN/m}$ and $\nu_{2D} \approx 0.6$ are in good agreement with all experimental observations, implying that the nonlinear effects are moderate. The resulting surface shear modulus [22] is $G_{2D} = K_{2D}(1 - \nu_{2D})/(1 + \nu_{2D}) \approx 125 \text{ mN/m}$. In Ref. [5], slightly larger values of 200–300 mN/m (obtained by interfacial shear rheology) are reported for similar OTS membranes.

In the case of HFBII, we can reduce the number of fit parameters by constraining $\nu_{2D} = 0.6$ to a value measured in an independent experiment [23] and determine the area compression modulus only. Fig. 2(b) shows that the area compression modulus K_{2D} increases for small deformations, where the capsule does not wrinkle (blue squares in Fig. 2(b)), to values around 500 mN/m. The onset of wrinkling coincides with a sharp increase of the modulus to a maximum value of $K_{2D} \approx 2000 \text{ mN/m}$. This sharp increase is consistent with the molecular structure of HFBII [24], which contains a rigid core consisting of four β -strands and is stabilized by disulfide bridges. The modulus K_{2D} increases sharply when compression of this rigid protein core sets in, while at small deformations, only contacts between hydrophobin proteins or a soft shell consisting of coil and loop structures surrounding the rigid β -barrel are compressed. The sharp rise of the compression modulus triggers wrinkling. Subsequently, the compression modulus decreases again (blue circles in Fig. 2(b)) likely signalling creep as also observed for the OTS capsules. Possible explanations for the creep behavior are the formation of microdefects such as shear cracks or localized bulges into the subphase, which weaken the hydrophobin layer.

The choice of the fixed value for ν_{2D} influences the absolute values obtained for K_{2D} and the size of its

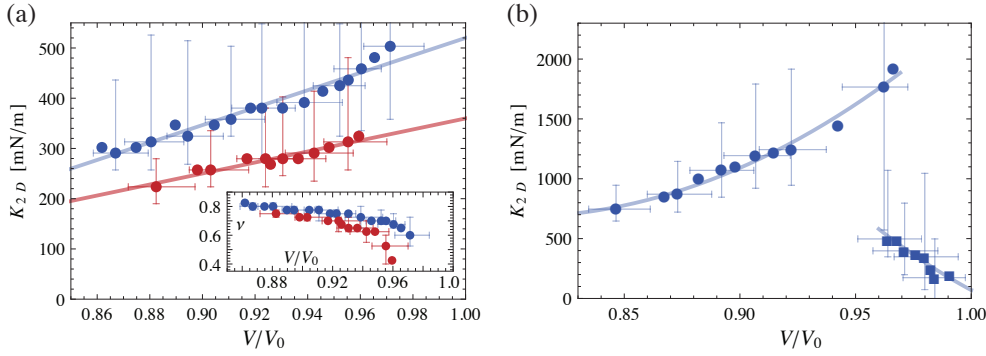


Figure 2: (Color online) Fit results for (a) an OTS capsule and (b) an HFBII capsule, with non-wrinkled (\blacksquare) and wrinkled (\bullet) shapes. Error bars were generated by displacing the sampling points about ± 1 pixel, see [19]. Lines are drawn to guide the eye. (a) Upper blue curve is for deflation, lower red curve for re-inflation. (b) For HFBII, the Poisson ratio was fixed to $\nu_{2D} = 0.6$.

jump when wrinkling sets in, while the characteristics described above are robust. Fits with free ν_{2D} are addressed in the Supplement [19].

The values $K_{2D} < 500$ mN/m for the compression modulus for small deformations and prior to wrinkling are in good agreement with values reported previously for HFBII [8, 25, 26]. The large values around $K_{2D} = 2000$ mN/m at the onset of wrinkling have not been reported before, since the experimental methods used in the literature are not reliable in the presence of wrinkles. However, a comparison to viral capsids consisting of densely packed proteins is possible. In Ref. [27], the bulk Young modulus of a viral capsid is measured as 1.8 GPa, which is comparable to our result for the bulk modulus $Y_{3D} = Y_{2D}/H_0 \approx 1$ GPa, where $H_0 \approx 2$ nm [28] is the hydrophobin layer thickness.

Finally, the wrinkling pattern shall be analyzed and be related to the bending stiffness. The wavelength of the wrinkles on the HFBII capsules cannot be measured directly: due to the low bending stiffness, the wavelength is too small to be resolved in the images. However, using eq. (3) with L_w , τ_s and $E_B = EH_0^3/12(1-\nu^2)$ obtained from the elastic fits, we expect wavelengths between 7.6 and 11 μ m. In the literature, similarly small or even smaller wrinkle wavelengths for compressed HFBII films in a Langmuir trough have been reported [17, 23, 26]. Note that the observable folds in Fig. 1(b) are not primary wrinkles, but rather secondary or higher order structures.

For OTS capsules, however, wrinkle wavelengths Λ may be determined from images with clearly visible wrinkles. The resulting bending stiffness is $E_B \approx (3.2 \pm 1.0) \cdot 10^{-14}$ Nm. Combining this value for E_B with measurements of Y_{2D} from the shape analysis we estimate the membrane thickness $H_0 \approx (0.84 \pm 0.09) \mu$ m, which is in approximate agreement with capsule thicknesses $0.86 < H_0 < 1.4 \mu$ m measured by electron microscopy [19]. Also the extent and position of the wrinkled region (see Fig. 1(a)) are in very good agreement with the experimental data.

In conclusion, the proposed theory for axisymmetric capsule shapes in the presence of wrinkling describes deflated experimental shapes of both OTS capsules and hy-

drophobin coated bubbles accurately. It is possible to fit the solutions of the shape equations to contours extracted from experimental images in order to find the elastic properties (area compression modulus and Poisson ratio) of the membrane. Additionally, a subsequent analysis of the wavelength of wrinkles which occur during the deflation can determine the membrane's bending stiffness. With this combination of analyses, the elastic properties of the capsule are completely characterized.

Applying this method to OTS capsules gives reasonable values for all three elastic constants – $K_{2D} \approx 500$ mN/m, $\nu_{2D} \approx 0.6$ and $E_B \approx 3.2 \cdot 10^{-14}$ Nm for the small deformation behavior. Furthermore, we observe a softening or creep of the capsules with decreasing volume, which we also observe for hydrophobin capsules.

For hydrophobin capsules, the area compression modulus initially grows upon deflation, $K_{2D} = 160$ mN/m to 500 mN/m. At the onset of wrinkling, it jumps to 2000 mN/m because compression of the rigid protein core sets in. We hope that these results will inspire future work on possible nonlinear elastic laws for HFBII membranes based on an elastic modulus which depends on the local stretches and diverges at a critical compression $\lambda_c < 1$.

These two applications prove the concept of the elastometry method, which could be added to the features of pendant drop tensiometers in the future. The method can reveal changes in elastic constants with decreasing volume that are not accessible by other methods. It can be further improved by using data from a simultaneous pressure measurement during deflation, which would eliminate one of the fit parameters.

SK and JK acknowledge financial support by the Mercator Research Center Ruhr (MERCUR). DV acknowledges support through Award no. KUK-C1-013-04, made by King Abdullah University of Science and Technology (KAUST). EA and PC thank Unilever Global Development Centre for the gift of hydrophobin and EPSRC and Unilever, plc for funding.

-
- [1] A. Fery and R. Weinkamer, *Polymer* **48**, 7221 (2007).
- [2] K. S. Chang and W. L. Olbricht, *J. Fluid. Mech.* **250**, 609 (1993).
- [3] G. Pieper, H. Rehage, and D. Barthès-Biesel, *J. Colloid Interface Sci.* **202**, 293 (1998).
- [4] W. Meier, *Chem. Soc. Rev.* **29**, 295 (2000).
- [5] H. Rehage, M. Husmann, and A. Walter, *Rheol. Acta* **41**, 292 (2002).
- [6] M. Husmann, Phd thesis, Universität Essen (2001).
- [7] R. Stanimirova, K. Marinova, S. Tcholakova, N. D. Denkov, S. D. Stoyanov, and E. Pelan, *Langmuir* **27**, 12486 (2011).
- [8] N. A. Alexandrov, K. G. Marinova, T. D. Gurkov, K. D. Danov, P. A. Kralchevsky, S. D. Stoyanov, T. B. Blijdenstein, L. N. Arnaudov, E. G. Pelan, and A. Lips, *J. Colloid Interface Sci.* **376**, 296 (2012).
- [9] P. Erni, H. A. Jerri, K. Wong, and A. Parker, *Soft Matter* **8**, 6958 (2012).
- [10] Y. Rotenberg, L. Boruvka, and A. Neumann, *J. Colloid Interface Sci.* **93**, 169 (1983).
- [11] E. Cerda and L. Mahadevan, *Phys. Rev. Lett.* **90**, 074302 (2003).
- [12] L. Landau and E. Lifshitz, *Fluid Mechanics* (Butterworth-Heinemann, 1987).
- [13] A. Libai and J. Simmonds, *The Nonlinear Theory of Elastic Shells* (Cambridge University Press, 1998).
- [14] S. Knoche and J. Kierfeld, *Phys. Rev. E* **84**, 046608 (2011).
- [15] B. Davidovitch, R. D. Schroll, D. Vella, M. Adda-Bedia, and E. Cerda, *Proc. Natl. Acad. Sci. USA* **108**, 18227 (2011).
- [16] D. Vella, A. Ajdari, A. Vaziri, and A. Boudaoud, *Phys. Rev. Lett.* **107**, 174301 (2011).
- [17] E. S. Basheva, P. A. Kralchevsky, N. C. Christov, K. D. Danov, S. D. Stoyanov, T. B. J. Blijdenstein, H.-J. Kim, E. G. Pelan, and A. Lips, *Langmuir* **27**, 2382 (2011).
- [18] H. King, R. D. Schroll, B. Davidovitch, and N. Menon, *Proc. Natl. Acad. Sci. USA* **109** (2012).
- [19] See supplemental material at [url will be inserted by publisher] for mathematical details.
- [20] L. Landau and E. Lifshitz, *Theory of Elasticity* (Butterworth-Heinemann, 1986).
- [21] E. Aumaitre, S. Knoche, P. Cicuta, and D. Vella, to appear in *Eur. Phys. J. E* (2013).
- [22] D. Barthès-Biesel, A. Diaz, and E. Dhenin, *J. Fluid Mech.* **460**, 211 (2002).
- [23] E. Aumaitre, Ph.D. thesis, University of Cambridge (2012).
- [24] J. Hakanpää, A. Paananen, S. Askolin, T. Nakari-Setälä, T. Parkkinen, M. Penttilä, M. B. Linder, and J. Rouvinen, *J. Biol. Chem.* **279**, 534 (2004).
- [25] A. R. Cox, F. Cagnol, A. B. Russell, and M. J. Izzard, *Langmuir* **23**, 7995 (2007).
- [26] T. B. J. Blijdenstein, P. W. N. de Groot, and S. D. Stoyanov, *Soft Matter* **6**, 1799 (2010).
- [27] I. L. Ivanovska, P. J. de Pablo, B. Ibarra, G. Sgalari, F. C. MacKintosh, J. L. Carrascosa, C. F. Schmidt, and G. J. L. Wuite, *Proc. Natl. Acad. Sci. USA* **101**, 7600 (2004).
- [28] K. Kisko, G. R. Szilvay, E. Vuorimaa, H. Lemmetyinen, M. B. Linder, M. Torkkeli, and R. Serimaa, *Langmuir* **25**, 1612 (2009).
- [29] This is a rough estimate, since the bulk Poisson ratio ν_{3D} is not necessarily equal to the membrane Poisson ratio ν_{2D} .

RECENT REPORTS

12/109	Dynamics of mechanically induced fiber reorientation in the material reinforced by two families of fibers	Melnik Goriely
12/110	Multiscale stochastic reaction-diffusion modelling: application to actin dynamics in filopodia	Erban Flegg Papoian
12/111	Exploiting the Synergy Between Carboplatin and ABT-737 in the Treatment of Ovarian Carcinomas	Jain Richardson Meyer-Hermann Byrne
12/112	The integration of hormonal signaling networks and mobile microRNAs is required for vascular patterning in Arabidopsis roots	Muraro Pound Help Lucas Chopard Byrne Godin Hodgman King Pridmore Helariutta Bennett Bishopp
12/113	Fast solution of Cahn-Hilliard Variational Inequalities using Implicit Time Discretization and Finite Elements	Bosch Stoll Benner
12/114	An Embedding Technique for the Solution of Reaction-Diffusion Equations on Algebraic Surfaces with Isolated Singularities	Rockstroh März Ruuth
12/115	Mathematicians at the Movies: Sherlock Holmes vs. Professor Moriarty	Moulton Goriely
13/01	Rotation, inversion, and perversion in anisotropic elastic cylindrical tubes and membranes	Goriely Tabor
13/02	Drop spreading and penetration into pre-wetted powders	Marston Sprittles Zhu Li Vakarelski Thoroddsen
13/03	On the mechanics of thin films and growing surfaces	Holland Kosmata Goriely Kuhl
13/04	Spatially Partitioned Embedded Runge-Kutta Methods	Ketcheson Macdonald Ruuth
13/05	Simple computation of reaction-diffusion processes on point clouds	Macdonald Merriman

13/09	Mathematical analysis of a model for the growth of the bovine corpus luteum	Prokopiou Byrne Jeffrey Robinson Mann Owen
13/10	Capillary deformations of bendable films	Schroll Adda-Bedia Cerde Huang Menon Russell Toga Vella Davidovitch
13/11	Twist and stretch of helices: All you need is Love	Đuričković Goriely Maddocks
13/12	Switch on, switch off: stiction in nanoelectromechanical switches	Wagner Vella
13/13	Pinning, de-pinning and re-pinning of a slowly varying rivulet	Paterson Wilson Duffy
13/14	Travelling-wave similarity solutions for a steadily translating slender dry patch in a thin fluid film	Yatim Duffy Wilson
13/15	A stochastic model for early placental development	Cotter Klika Kimpton Collins Heazell
13/16	Experimentally-calibrated population of models predicts and explains inter-subject variability in cardiac cellular electrophysiology	Britton Bueno-Orovio Van Ammel Lu Towart Gallacher Rodriguez

**Copies of these, and any other OCCAM reports can be obtained from:
Oxford Centre for Collaborative Applied Mathematics**

**Mathematical Institute
24 - 29 St Giles'
Oxford
OX1 3LB
England
www.maths.ox.ac.uk/occam**